Wear of poly (methyl methacrylate) against a metallic surface in dry conditions

Jean Geringer, Bernard Forest, Pierre Combrade

Wear of poly (methyl methacrylate) against a metallic surface in dry conditions

Jean Geringer, Bernard Forest, Pierre Combrade

Jean Geringer[a], Bernard Forest[a], Pierre Combrade[b]

[a] *Ecole Nationale Supérieure des Mines de Saint-Etienne, UMR CNRS 5146, 158, cours Fauriel F-42023 Saint-Etienne Cedex 2*
Tel: (33).4.77.42.66.88, Fax: (33).4.77.42.01.57, E-mail: geringer@emse.fr
[b] *Centre technique Framatome-ANP 1, rue B. Marcet F-71205 Le Creusot Cedex*

Abstract

Wear of Poly (Methyl MethAcrylate), PMMA, against a metallic surface, AISI 316L stainless steel, SS, has been investigated in dry conditions. These materials have been used to simulate the degradation of the contact, femoral stem-bone cement in the field of hip prosthesis. First of all, no significant wear was observed on the 316L SS. PMMA wear has been quantified: the energy wear coefficient, slope of the line, and wear volume according to the cumulated dissipated energy, don't depend on the normal load, F_N. This energy analysis allows predicting the PMMA wear depth. According to the comparison between the measured dissipated energy and the energy breaking polymer chains, mechanical dissipated energy is used essentially to transform third body structure and to expel it from the contact between the two materials. Moreover, the experimental results have highlighted the stick-slip phenomenon. Lastly, Attenuated Total Reflectance-Fourier Transform InfraRed, ATR-FTIR, and Reflection Absorption-Fourier Transform InfraRed, RA-FTIR have shown that PMMA debris configuration and conformation have changed after wear against 316L SS. The driving force of these changes seems to be the acid-base interactions between PMMA and hydroxyl groups of the stainless steel surface.

Keywords: friction, wear, PMMA, dissipated energy, stick-slip phenomenon.

INTRODUCTION

This work aims at studying specific wear: fretting, friction under small displacement, when the displacement is lower than the contact width between the two materials. This phenomenon is a significant problem in some industrial fields. Particularly, polymers degradations due to fretting are involved in automobile industry [1]. Many polymers materials have been investigated in fretting conditions like Polypropylene/acrylic resin [1], PMMA plate/stainless steel ball [2] or PMMA flat sample/glass cylinder [3].

The wear in fretting conditions presents specific characteristics compared to these in friction conditions. Indeed, as the imposed displacement is lower than the contact width, a confined zone appears inside the contact. The created debris are called the third body. Its creation and evolution over time does depend on the contact geometry, on the normal load and on the value of the imposed displacement. Different fretting regimes have been identified according to the normal load and the imposed displacement: stick, partial slip and gross slip [4,5]. Moreover, materials degradation depends on these several fretting regimes.

Particularly, this work is devoted to the study of fretting that occurs between femoral stem, made of stainless steel in this particular case, and bone cement, made of PMMA principally, when a cemented hip prosthesis is implanted. In fact, hip prosthesis can be implanted following two ways. On the one hand, the prosthesis is inserted directly in the femoral bone, on the other hand it can be inserted using bone cement. Why studying fretting ? Because this specific friction is one of the main factors of aseptic loosening due to debris generation that causes inflammation reactions.

Generally, this degradation occurs in a physiological liquid containing blood, proteins, cells, etc. However, dry zones can appear where friction between femoral stem and bone cement occurs. Moreover, as bone cement is principally made of PMMA, it has been decided to use a model component: transparent PMMA to follow live fretting degradation.

Fretting has been studied in dry conditions, between a cylinder sample made of PMMA and a plate sample made of 316L stainless steel. The normal loads (from 2.83 $N.mm^{-1}$ to 11.33 $N.mm^{-1}$) and the imposed displacement ($\pm$ 40 µm) allow the simulation of the gross slip regime for the considered contact [6]. Two distinct stages can be observed, Fig. 1: the first is the elastic accommodation between the two materials in contact and the second is the friction characterized by a plateau that corresponds to a constant value of tangential load. However, during this sliding phase, friction of PMMA can be irregular because of instabilities. This phenomenon is called stick-slip. In the fretting case, the stick-slip has been already observed between aluminium alloys [7] or PMMA samples [8]. This process provides

a particular PMMA degradation. Consequently, PMMA debris are produced by friction during stick-slip with stainless steel. Physically, they are generated by the energy dissipated during fretting, measured as the area of the cycle tangential load vs. imposed displacement, Fig. 1.

This study will focus on three precise aspects of the fretting degradation. First, wear will be investigated quantitatively. The aim is to determine which physical parameter is judicious to quantify wear. Thus, the adhesion influence will be studied considering the Fuller-Tabor parameter related to the wear process. Second, thanks to a specific device, the in situ observation will allow following wear degradation. Moreover, this information will be corroborated with other observation methods. The main question is: what is the wear shape of PMMA ? Third, it will be very interesting to know whether PMMA debris suffer significant structural transformations, configuration and conformation [9-11], due to wear.

EXPERIMENTAL

Materials

Stainless steel 316L (Z2CND17-12) has improved cleanliness and very low carbon content. The chemical composition is shown in Table 1. The 316L samples dimensions were 9 mm × 9 mm × 20 mm, Fig. 2. The friction plane surface was polished with diamond paste down to 0.25 µm and, finally, with colloidal silica with a granulometry lower than 0.06 µm. The measured roughness, Ra parameter, was lower than 0.05 µm, the length of measurements was equal to 6 mm. The used apparatus was a Talysurf® profilometer. After polishing, 316L samples were cleaned, during 10 minutes, with ethanol in an ultrasonic cleaner, then dried in ambient air and conserved in vacuum environment to avoid atmosphere pollution.

PMMA, Perspex®, is an optically transparent thermoplastic material. This transparency has allowed observing *in situ* degradations of PMMA during fretting. At room temperature, it is a hard and brittle material. The cylindrical samples of PMMA had the following constant dimensions concerning the parallelepipeds shape: 9 mm × 9 mm × 15 mm, Fig. 2. Consequently, the contact length was equal to 15 mm. The curvature radius of the cylinder was equal to 10 mm. PMMA samples were polished with Altuglass Polish 1 and 2®. Then, they were cleaned with soap Neutracon Deacon®, rinsed with water and conserved in vacuum environment.

Table 2 shows the PMMA properties before fretting. Tacticity was established by 1H NMR spectroscopy in 100 % CDCl3 solutions at 333 K. Brückner spectrometer operating at 300 MHz was used. Molecular weights and polydispersity have been investigated by size exclusion chromatography, solvent was tetrahydrofuran (HPLC grade), using a Waters chromatograph calibrated with PMMA standards. An Ubbelhode viscosimeter, tube diameter equal to 0.53 mm, at controlled temperature 293 K, was used to determine the intrinsic viscosity. The solvent was toluene (HPLC grade) and it was filtered under vacuum before use. The concentrations of PMMA solutions were within the range of 1 $g.L^{-1}$ to 6 $g.L^{-1}$. The duration of displacement, in the toluene solution was always lower than 400 s. Three measurements have been made to obtain representative accuracy. At last, Setaram DSC 131 apparatus was used to determine Tg, glass transition temperature. The temperature program consisted of three stages: the first stage lasted 1,000 seconds at room temperature, the second was the temperature increase with a gradient equal to 20 $°C.min^{-1}$ during 460 seconds and the third was a temperature decrease with a gradient equal to -20 $°C.min^{-1}$. The measurement atmosphere was composed of pure nitrogen.

Experimental and observations device

The fretting experiments have been investigated by a Tribomines® device installed on a Schenck-PSA 10 servo hydraulic traction-compression machine. An arm fixed on a ball bearing allowed the application of a normal load, F_N, within the range of 2.83 $N.mm^{-1}$ to 11.33 $N.mm^{-1}$, between both materials in contact, Fig. 3. The hydraulic actuator, controlled by two LVDT gauges, controlled the sinusoidal displacements, with an amplitude equal to ± 40 µm. The tangential load is recorded thanks to a load sensor Kistler® 9041A SN 371493. Displacements and tangential loads were monitored and recorded (frequency of recording = 300 Hz) using Testpoint® software. Tests were performed at room temperature. The relative humidity was approximately equal to 50 %.

In this study a cylinder/plane contact has been used, with a contact length of 15 mm. The cylindrical sample (white stripe on Fig. 3) was mounted on a fixed component with a conical aperture through which the contact observation was possible. The plane sample (black on Fig. 3) was fixed on a ball joint that allows a careful adjustement of the contact between specimens. The frequency of the imposed displacement was equal to 1 Hz.

PMMA transparency allowed the continuous observation and recording of the contact through the specimen with magnifications within the range of ×75 to ×300.

After fretting experiments, PMMA samples and debris on stainless steel surface have been observed with a Scanning Electron Microscope equipped with a Field Electron Gun (SEM-FEG) JEOL 6500. This SEM-FEG apparatus has been used because the source potential is weaker than that of the classical SEM apparatus. Indeed, PMMA surface is transformed during the observations when the source potential is too high.

3D images of PMMA and wear volume measurements have been obtained with a mechanical profilometer, Somicronic® used with Surfascan® software. The accuracy of these last measurements was estimated to be 10 %.

Infrared spectroscopy

Two FTIR devices have been used to investigate the transformations of PMMA debris on stainless steel surface and PMMA sample surface. Indeed, in order to obtain vibration bands of debris Reflection Absorption-Fourier Transform InfraRed, RA-FTIR, device was the most appropriate infrared apparatus because the debris size was lower than 2 µm and the reflection quality of the polished 316L surface is high. The ATR-FTIR device gave the more significant spectrum concerning the surface of PMMA sample after fretting tests.

RA-FTIR spectroscopy was performed using Spectrum GX Systems Perkin Elmer. The detector was constituted by a FR-DGTS Mid-IR (KBr) with a sensibility window within the range of 7,000 to 370 cm^{-1}. For each spectrum acquisition, 256 scans were performed to increase the signal to noise ratio. The device resolution was approximately 0.3 cm^{-1}. The reflection angle of the incident beam was 70°. With this method, the carbonyl band vibration was particularly focused. A Lorentzian band shape allowed fitting this vibration. In fact, this band is related to the absorption of free and bonded carbonyl function of PMMA due to interactions with others organic functions on the 316L surface.

ATR-FTIR was performed using FTS 185 Biorad spectrometer. This specific device implies the use of the golden gate simple reflection Specac P/N 10500 platform. Each spectrum was an average of 256 scans. The ATR crystal was diamond and thus made possible the analyze of PMMA surface sample. The analyzed depth was within the range of 25 µm (wave number, $\bar{\nu}$, equal to 400 cm^{-1}) to 2.5 µm ($\bar{\nu}$ equal to 4,000 cm^{-1}). The resolution was equal to 4 cm^{-1}.

The baseline signal has been recorded before each spectrum in order to obtain the best sensibility. For each test condition, five measurements were carried out on the 316L surface to

analyze PMMA debris and to measure the absorbance values necessary to interpret structure changes. The same procedure was used on PMMA sample surface.

RESULTS AND DISCUSSION

Wear and dissipated energy

Fretting tests were carried out for different durations. It became possible to determine the wear volume evolution. The first wonder is to know if this wear volume depends on time or on other physical parameters. Consequently, wear volume was drawn according to the time and the cumulated dissipated energy, sum of the dissipated energy for all number of cycles. Fig. 4 shows, for $F_N = 5.67$ N.mm^{-1}, the linear evolution of the wear volume according to the cumulated dissipated energy. Table 3 presents the values of the time and energy wear coefficient, slope wear volume vs. time and vs. cumulated dissipated energy, respectively. PMMA wear is correlated to the cumulated dissipated energy. The wear depth was measured with the mechanical profilometer, Fig. 5. The wear depth is proportional to the cumulated dissipated energy, therefore the PMMA wear is related to the dissipated energy during fretting.

From this first result, we can compare values of the energy wear coefficient with the carbon-carbon bond energy, $D_{(C-C)}$, in order to know if the dissipated energy is used to break the polymer chains. First of all, a molar energy wear coefficient has to be defined:

$$\varphi_{mol} = \frac{M}{\alpha_V \rho} \quad (1).$$

M: molar weight of a constitutive unit (monomeric unit),

α_V: energy wear coefficient,

ρ: specific gravity, considered as a constant during wear.

One considers that all the dissipated energy during wear is used to break polymer chains. If this attempt is right, the ratio, φ_{mol}, would correspond to the carbon-carbon bond. However, Table 4 indicates that the ratio $\varphi_{mol}/D_{(C-C)}$ is higher than 1,000. Hence, the dissipated energy is not used to break the polymer chains. We can conclude that the dissipated energy is used principally to mix and transform the third body and to expel PMMA debris out of the contact zone. Polymer chains breaking is not the main phenomenon of PMMA debris

generation. This result has been highlighted for a contact steel/TiN [12]. The energy wear coefficient has to be interpreted with the use of other physical factors. The adhesion could be responsible for consuming energy during fretting. The Fuller-Tabor parameter, θ, is defined as a ratio between partition load due to asperities and load due to adhesion,

$$\theta = \frac{E^* z^{3/2} b^{1/2}}{bw} \quad (2)$$

$z = 75.10^{-9}$ m: separation of average lines of two bodies [13],
$b = 3.10^{-6}$ µm: curvature radius of asperities (estimated values from 3D mechanical profilometer),
$w = 2.5.10^{-2}$ J.m^{-2}: Dupré energy (estimated value),
$E^* = 2.91.10^9$ Pa: effective Young modulus, $E^* = ((1-\nu_1^2)/E_1 + (1-\nu_2^2)/E_2)^{-1}$,
ν_1 and ν_2: Poisson ratios,
E_1 and E_2: Young moduli; 1 refers to PMMA and 2 refers to 316L SS [14,15].

As two phenomena are involved in friction, adhesion and separation load, the Fuller-Tabor parameter has an influence in the wear energy coefficient. We have considered the product $D_{(C\text{-}C)}*\theta$ equal to φ_{mol}. Table 5 presents a comparison between the wear energy coefficient calculated with the Fuller-Tabor parameter and the one obtained experimentally. These two values are in good agreement. Of course, z, b and w have to be confirmed by experiments but φ_{mol}, as it has been defined, corresponds to an acceptable physical value of the wear energy coefficient. However, the proposed approach rules out the heat transfer. Experimentally, we have tried to monitor temperature increase of PMMA thanks to a thermocouple during friction and IR camera. Unfortunately, no significant results could be derived. One might expect that a part of the dissipated energy could account for heating the material, especially the asperities on the surface. However the temperature increase is too short to measure it with accuracy. Other investigations have to be carried out to obtain information about this phenomenon.

Stick-slip phenomenon

A fretting cycle, tangential load vs. imposed displacement, shows two parts: an elastic slope and a friction plateau, Fig. 1. However, a precise analysis of the friction plateau

highlights that the tangential load is not constant. Due to the stick-slip phenomenon, adhesion and friction alternation, the tangential load varies according to time, Fig. 6. It is worth noting that the results below depend on the frequency of recording, i.e. 300 Hz, and on the stiffness of the tangential load sensor. These parameters have been considered as constant during experiments.

Hence, the stick-slip amplitude, β_1 (difference between the maximum and minimum of the tangential load on the friction plateau), and the stick-slip coefficient, β_2 (ratio between β_1 and the contact length), is in relation with the variations of stick-slip according to the applied normal load. Fig. 7 a) shows the stick-slip coefficient according to the number of cycles for two tests, i.e. normal loads equal to 11.33 $N.mm^{-1}$ and 2.83 $N.mm^{-1}$. Hence, the stick-slip phenomenon depends on the normal load. Fig. 7 b) shows the β_2 coefficient variation according to the normal load per contact length. β_2 has been calculated when the number of cycles was equal to 80,000. β_2 is the average value of three different experiments. At the beginning of the test, experimental data are scattered. This fact is explained by the running-in period of wear. When the generation of debris starts the stick-slip phenomenon is disturbed. In our tests conditions, the contact length is equal to the PMMA sample length, which is the shortest dimension, i.e. 15 mm. First, these stick slip coefficients values are in the same range than for a contact PMMA/glass [16]. Second, these coefficients increase linearly according to the normal load per contact length. It seems that the stick-slip is more important when the normal load increases.

An acoustic emission was audible during fretting tests in dry conditions. This sound is characteristic of the stick-slip phenomenon. In order to explain the normal load influence on the β_2 coefficient, we can report results from previous studies made with a contact PMMA/PMMA [17]. When the normal load increases, and consequently so is the normal pressure, the PMMA asperities suffer plastic and viscoelastic deformations. Accordingly, the contact area and the adhesion forces increase. The stick time follows the same variation. During this stick stage, the elastic energy is stored in the smooth material, the tangential load is the highest. Afterwards, during the slip stage, the elastic energy is released. Consequently, the measured tangential load is the lowest. The alternation of these two stages, stick and slip, accounts for the tangential load changes on the friction plateau. The end of the slip phenomenon can be related to the elastic energy quantity. If this released energy tends towards zero, the stick stage starts again.

Fig. 7 a) also shows that the stick-slip phenomenon is not steady, β_2 accuracy is weak. Indeed, elastic bounces were identified during friction of PMMA against PMMA. The random

occurrence of these bounces could be due to brief contacts of PMMA particular asperities [18]. Accordingly, the β_2 values changes are random. Moreover, the amplitude depends on the stick stage efficiency. Due to the PMMA roughness and the third body flow between the two materials in contact, the stick could not be a steady state phenomenon. However, Fig. 7 b) highlights that the normal load accounts for the increase of the stick-slip coefficient. The average β_2 increases linearly vs. F_N, normal load divided by contact length, i.e. 15 mm, with a correlation coefficient close to 1. One can consider that the stick stage is more efficient when the normal load, or the pressure, are the highest. The stick-slip evolution depends on PMMA debris, third body, but also produces debris. The elastic energy is only stored and released, it has no influence on the measured dissipated energy that is therefore used to deform plastically, to break PMMA asperities and to transform the debris. After this mechanical study, 2D and 3D images and SEM observations give details on the debris evolution during fretting.

Observations of PMMA degradations during fretting

2D images

The specific device, with a camera, allows observing *in situ* PMMA debris generation and evolution according to time. The 2D images will be compared with the dissipated energy evolution according to time, Fig. 8. This figure shows the dissipated energy vs. time for two tests where F_N = 11.33 N.mm^{-1}, one for 30,000 cycles and the second for 80,000 cycles. It shows that dissipated energy is not constant.

Fig. 9 highlights these PMMA degradations for a test duration lower than 500 seconds. First of all, the brilliant zones at the edges of the contact represent the PMMA debris. At the beginning of fretting, debris are produced at these edges where the Von Mises equivalent stress and the hydrostatic pressure are maximum periodically [19,20]. Hence, the PMMA behavior is not elastic, the stress passes the Von Mises stress criterion and as PMMA is ductile material, debris generation starts. When F_N is equal to 2.83 N.mm^{-1} (images on top Fig. 9), debris are easily expelled from the contact, which is not the case for the highest loads, i.e. when F_N is higher or equal to 5.67 N.mm^{-1}. For these high loads, the first interferences fringe, at the edge of the contact, is deformed. It is the evidence of PMMA degradation at the edge of the contact. Despite this wear zone, debris are not expelled easily out of the contact zone. Thus, the contact pressure is the preponderant factor to explain that debris stay inside

the contact zone. At last, for the observations with duration lower than 500 seconds, images show that PMMA debris are stuck on the 316L surface, Fig. 9. 316L sample moves and the PMMA sample is fixed. The movie of fretting test shows that these debris move with the metal sample. Accordingly, it exists stuck zones between 316L and PMMA. This observation agrees with the stick-slip phenomenon where, after the stick stage, debris are produced. To summarize these degradations, Fig. 10 proposes two different mechanisms according to the normal load. When the normal load is higher than 2.83 $N.mm^{-1}$, the contact pressure is high and PMMA debris ejection is avoided for this first stage. Images obtained when F_N is equal to 8.5 $N.mm^{-1}$ and 11.33 $N.mm^{-1}$ show the same behavior than for F_N of 5.67 $N.mm^{-1}$ in this first stage of fretting process. These 500 first seconds contain stick and slip stages that involve a dissipated energy increase, range 1 on the Fig. 8.

Fig. 11 presents images for a duration within the range from 1,000 seconds to 60,000 seconds. A comparison can be led between these images and the dissipated energy evolution, Fig. 8. The behavior is the same for all applied normal loads. The second range, Fig. 8, corresponds to a decrease of the dissipated energy. PMMA debris are produced during fretting, they constitute the third body that protects the bulk material; hence a protective layer involves a decrease of the dissipated energy. Moreover, adhesion between 316L and PMMA becomes more difficult. However, for F_N higher than 2.83 $N.mm^{-1}$, stuck zones appear at the contact center. One might expect that this zone will be less worn than the edge of the contact. Due to the debris inside the contact, the contact pressure maximum moves from the contact center to the edges because the zone between the center and the edge, which contains debris, bears most of the normal load [21]. Stuck PMMA debris are always on the metal surface, Fig. 11 (images 4,500 and 15,000 cycles, F_N = 2.83 $N.mm^{-1}$ and 8.5 $N.mm^{-1}$). They could increase the PMMA wear like an ‘awl’. For the highest normal loads values, slip can start abruptly randomly, proof of the stick-slip presence. At last, the third stage, Fig. 8, corresponds to a relatively constant dissipated energy. The flow of PMMA debris reaches a relative steady state despite the stick-slip phenomenon.

Two tendencies are important from these 2D images: the most worn zones are probably at the edge of the contact and generated debris are transformed differently if they are stuck on metal surface (they constitute the third body) or expelled out of the contact zone. The 3D images will allow knowing if the most worn zones are at the edge of the contact.

3D images and SEM observations

From Fig. 12, two different wear shapes can be observed. Indeed, when the normal load is equal to 2.83 $N.mm^{-1}$, wear is relatively uniform, like a 'U' shape wear track area. On the contrary to the highest normal loads, the wear track area has a 'W' shape. The assumptions made in the previous part seem to be right. Indeed, the wear is the most important at the edge of the contact. This confirms that the two materials in contact are either stuck or very close. For the highest load, F_N = 11.33 $N.mm^{-1}$, the depth is the most important. It is due to the increase of the hydrostatic pressure that accounts for the crazing and the debris generation. Moreover, grooves can be distinguished on the 3D images. PMMA debris stuck on the 316L could account for these grooves that are the most important when the normal load increases.

Fig. 13 shows SEM images for F_N = 5.67 $N.mm^{-1}$. The image a) of this figure shows half a contact zone where the upper part is the edge of the contact and the lower part is the center of the contact. The image b) shows plastic zone on PMMA highlighted by the presence of steps characteristic of plastic deformation. This image corresponds to the deepest zones in the 'W' shape wear track area. The image c) represents PMMA debris that are compacted by fretting at the contact center. One can consider that this smooth area is the same than the one observed in the 2D images, Fig. 11, contact without debris, 15,000 cycles, F_N equal to 5.67 $N.mm^{-1}$. PMMA and 316L stainless steel are very close. Why are these samples able to slip and, moreover, why is this zone less worn ? The image d) is a magnification of this area. Cracks are present and allow the slip in addition to the less wear ratio compared to the edge of the contact.

Two images show the main difference between the contact center for the lowest normal load used, i.e. 2.83 $N.mm^{-1}$, and the higher normal loads, Fig. 14. In fact, when F_N is equal to 2.83 $N.mm^{-1}$, deep cracks are present at the contact center, on the contrary to higher normal loads. Indeed, wavy scales can be observed. Consequently, the motion of samples is possible without an excessive wear at the center.

To conclude on this observations part, the third body behavior is multiple. PMMA debris are produced. Then they can be expelled out of the contact zone or stay inside and be compacted. Wavy scales are also at the contact center, for normal loads higher than 2.83 $N.mm^{-1}$. Moreover, the protective role of the third body is effective. It is interesting to note that the stick-slip phenomenon is not synonymous of the important wear in dry fretting

conditions because PMMA debris are stuck on the 316L. Wear is effective when debris are expelled out of the contact zone.

NB: Test conditions of this study were in dry conditions. The same experiments have been carried out in liquid medium (solution containing high chlorides concentration, Ringer solution, to simulate physiological liquid). The goal was to take into account potential liquid influence on the fretting degradation between PMMA and stainless steel. Main differences between dry and wet conditions exist. On the one hand, 316L suffers significant degradation, the energy wear coefficient of 316L was almost three times higher than the energy wear coefficient of PMMA. On the other hand, wear shapes were totally different. In wet conditions, PMMA exhibits a 'U' wear shape and 316L a 'W' wear shape. In dry conditions, PMMA exhibits a 'W' wear shape and 316L does not suffer significant degradation [14,22]. The specific 'W' wear shape of 316L, in aqueous medium, is attributed to a local crevice corrosion mechanism.

In the next part, in dry conditions, infrared investigations confirmed by NMR and DSC give interesting details on the configuration and conformation evolution of the PMMA debris.

Configuration and conformation of PMMA debris

Carbonyl bond evolution

In the previous part, it has been noted that PMMA debris were stuck on the metal surface. To conclude if bonds between PMMA and 316L surface are actual, RA-FTIR has been investigated to follow the characteristic carbonyl bond, i.e. between 1748 and 1728 cm^{-1}, values of waves number. Indeed, the vibration of the free carbonyls stretching corresponds to a waves number equal to 1748 cm^{-1} and that of the bonded carbonyls stretching to a waves number equal to 1728 cm^{-1}. Fig. 15 a) shows the spectrum obtained from a PMMA reference sample, the waves number of the carbonyl bond is equal to 1748 cm^{-1} and from PMMA debris, the waves number of the bonded carbonyls with groups on the 316L surface equal to 1728 cm^{-1}.

Fig. 15 b) represents the bonded carbonyls ratio according to the applied normal load. This ratio, $f_{C=O}^{bonded}$ is calculated like this:

$$f_{C=O}^{bonded} = \frac{A_{C=O}^{bonded}}{A_{C=O}^{bonded} + \frac{\varepsilon_{C=O}^{bonded}}{\varepsilon_{C=O}^{free}} A_{C=O}^{free}} \quad (3).$$

Deconvolution analysis has allowed calculating the absorbance for the different waves number. *free* indication corresponds to free carbonyls stretching vibrations and *bonded* indication corresponds to bonded carbonyls stretching vibrations. *A* is the absorbance and ε is the molar extinction coefficient. In first approximation, $\varepsilon^{bonded}/\varepsilon^{free}$ is considered equal to 1 [9]. A^{free} and A^{bonded} are measured experimentally. It is worth noting that the ratio, $f_{C=O}^{bonded}$, increases according to the normal load until F_N of 8.5 N.mm^{-1}. Accordingly, the acid-base interactions are more important if the normal load increases. The stick-slip phenomenon induces stuck debris on the metal surface and, obviously, the acid-base interactions proportion increases. As PMMA debris are less stuck at lowest normal load, debris are more expelled out of the contact zone, this fact has been observed thanks to the 2D images. However, the ratio, $f_{C=O}^{bonded}$, decreases when F_N is equal to 11.33 N.mm^{-1}. As the tangential load increases with the normal load, one can assume that the debris ejection becomes preponderant once again. Moreover, the acid-base interactions are more preponderant for the syndiotactic configuration [23]. The next analysis, between 1350 cm^{-1} and 1100 cm^{-1}, will be discussed in order to confirm or not this assumption, i.e. that the syndiotactic configuration ratio increases.

Range 1350 cm^{-1} – 1150 cm^{-1}

The four vibrations of this range vary according to the PMMA configuration. It corresponds to the C-O-CH_3 vibration. Fig. 16 shows that the spectrum from PMMA reference and that from worn PMMA are different. The comparison of these two spectra implies that the syndiotactic configuration seems to increase after fretting test [24]. As the configuration has been modified, the bonds of the backbone have been broken. Indeed, a part of the dissipated energy during fretting is effectively used to break carbon-carbon bond. This energy fraction stays low compared to the values of the measured dissipated energy.

Table 6 is obtained by DSC measurements for two PMMA samples types: four are relative to a polished sample and the fifth is relative to PMMA debris obtained after 1,620,000 seconds. Just one test was investigated due to this long duration necessary to obtain a sufficient weight. One can consider that the glass transition temperature increases over time. It indicates that the ratio of the syndiotactic configuration grows after fretting tests [25].

NMR spectrum can confirm that this syndiotactic configuration increases. Table 7 presents the configuration comparison between the reference PMMA and debris obtained during fretting for a duration equal to 1,620,000 seconds. Each shift corresponds to a signal which comes from a precise configuration. We can conclude that the syndiotactic configuration ratio increases after fretting test. Once again, due to test duration, only one test was carried out. The obtained values only give a tendency confirmed by DSC and IR analysis.

At last, the ratio between the absorbance measured at 1240 cm^{-1} and at 1270 cm^{-1} is presented Fig. 16 b). In fact it represents the ratio between backbone conformation energy and the total conformation energy that is equal to the sum of backbone and side-chain conformation energies. If this ratio increases, this is because of the interaction of PMMA with a surface [25]. For a syndiotactic configuration, this ratio increases in order to improve adhesion of debris on the metal surface. Indeed, ester groups are alternatively arranged along the backbone chain and it needs additional conformational energy to make possible the adhesion. Fig. 16 b) shows that the backbone energy increases according to the normal load and decreases weakly when F_N is equal to 11.33 $N.mm^{-1}$.

To sum up, the syndiotactic configuration ratio increases according to the normal load. Different analyses confirm this increase. The driving force of this configuration change can be attributed to the acid-base interactions between carbonyl function of PMMA and surface groups of stainless steel. When F_N is maximum, i.e. equal to 11.33 $N.mm^{-1}$, the syndiotactic configuration seems to decrease due to the important dissipated energy that prevents the adhesion of PMMA.

Range 900 cm^{-1} – 800 cm^{-1}

RA-FTIR experiments, for this spectrum range, did not produce a sufficient absorbance. Moreover, ATR-FTIR could not be used to analyse PMMA debris because the thickness of the debris was too low. This is the reason why ATR-IRTF was used to analyze worn PMMA surface.

In this spectrum range, the 860 cm^{-1} peak corresponds to a vibration due to the trans-trans conformation related to syndiotactic configuration and the helix conformation. The 840 cm^{-1} peak corresponds to the trans-gauche conformation [10]. Fig. 17 a) exhibits the spectrum of PMMA reference and b) worn PMMA surface. The main difference is the peak apparition at 860 cm^{-1}, which corresponds to the trans-trans conformation. On the contrary to the other spectrum range, no variation of the ratio between the absorbance at 860 cm^{-1} and 840 cm^{-1}

was significant according to the normal load. Moreover, the evolution of this ratio was also investigated through time, Fig. 18. The trans-trans conformation ratio increases on the worn PMMA surface. This change confirms the previous assumption: the syndiotactic configuration ratio compared to the others increases during fretting wear. One might expect that the helix conformation involves an optimum contact between the PMMA ester group and the groups like hydroxyls on the metal surface. Fig. 19 proposes a possible structure of the helix structure which corresponds to the syndiotactic configuration and the main difference with the trans-gauche conformation that is related to the isotactic configuration.

CONCLUSION

The fretting between PMMA sample and stainless steel has been investigated. The PMMA wear volume has been found to be proportional to the dissipated energy during fretting. A molar energy wear coefficient has been defined according to the carbon-carbon bond energy and the Fuller Tabor parameter. Wear energy coefficients calculated with this value and measured were in good agreement. The stick-slip phenomenon was highlighted, it increases with the applied normal load. Plastic or viscoelastic deformations could account for the debris generation.

Continuous observations, 2D images, post mortem images, and 3D images, have highlighted two different behaviors dependant on the normal load. When F_N was equal to 2.83 $N.mm^{-1}$, debris were expelled easily from the contact zone. A 'U' wear shape was found because wear was approximately homogeneous on the whole contact area. SEM observations showed that deep cracks allowed debris generation. For higher loads, debris stayed inside the contact and could be stuck on the metal surface. Wavy scales accounted for the motion accommodation. The third body could protect the bulk PMMA. Finally, for higher loads, the worn zone highlighted a particular ‘W’ wear shape.

The driving force of the debris adhesion was the acid-base interaction on the metal surface. Moreover, the syndiotactic configuration ratio increased in comparison with the other configurations. Thus, the helix conformation, corresponding to the syndiotactic configuration, grew and the interaction between PMMA carbonyl function and groups on the 316L surface was more efficient than in the case of the trans-gauche conformation. This particular transformation of debris occurs on the metal surface and highlights the different behavior between bulk PMMA and debris PMMA.

ACKNOWLEDGEMENTS

The authors are grateful to M. Dursapt and A. Jourani for the access to the 3-D profilometer at the ENISE (National School of Engineers at Saint-Etienne), to Professor C. Carrot for the Ubbelhode viscosimeter use, the molecular weights measurements and writing advices at LRMP, laboratory of the Jean Monnet University. The ^{1}H NMR Brückner apparatus use has been possible thanks to C. Lucas and F. Lefebvre, LCOMS, laboratory of CPE (School of Engineers at Lyon). Lastly, the RA-FTIR acquisitions has been carried out at Framatome-ANP, corrosion and chemistry department, Le Creusot.

REFERENCES

1. N. Eiss , J. Hanchi, *Tribology International*, **31**, 653 (1998)..

2. B.J. Briscoe, A. Chateauminois, T.C. Lindley, D. Parsonage, *Tribology International*, **31**, 701 (1998).

3. A. Krichen, C. Bradai, A. Chateauminois, M. Kharrat,. *Wear*, **230**, 146 (1999).

4. O. Vingsbo, S. Söderberg, *Wear*, **126**, 131 (1988).

5. O. Vingsbo, J. Schön, *Wear*, **162-164**, 347 (1993).

6. J. Geringer, B. Forest, P. Combrade, *Wear Analysis of materials used as orthopaedic implants in two media: air and Ringer solution*, Proceedings, Eurocorr 2004, Nice.

7. Z.R. Zhou, *Fissuration induite en petits débattements : application au cas d'alliages d'aluminium aéronautiques*, Ecole Centrale de Lyon Thesis 1997, n° 92-50.

8. S. Bouissou, J.P. Petit, M. Barquins, *Wear*, **214**, 156 (1998).

9. F.M. Fowkes, *J. Adh. Sci. Tech.*, **1**, 7 (1987).

10. Y. Grohens, M. Brogly, C. Labbe, J. Schultz, *Polymer*, **38**, 5913 (1997).

11. J. Chen , G. Zheng, L. Xu, J. Zhang, Y. Lu, G. Xue, Y. Yang, *Polymer*, **42**, 4459 (2001).

12. S. Fouvry, T. Liskiewicz, P. Kapsa, S. Hannel, E. Sauger, *Wear*, **255**, 287 (2003).

13. F. Robbe-Valloire, *Wear*, **249**, 286 (2001).

14. J. Geringer, B. Forest, P. Combrade, *Wear*, **259**, 943 (2005).

15. K.N.G. Fuller, D. Tabor, *Proc. R. Soc. London*, **Ser. A**, 327 (1975).

16. A. Krichen, *Simulation numérique et analyse expérimentale du comportement d'un contact verre/PMMA sous sollicitation de fretting*, Ecole Centrale de Lyon Thesis 1997, n°97-21.

17. S. Bouissou, J.P. Petit, M. Barquins, *Wear*, **215**, 137 (1998).

18. S. Bouissou, J.P. Petit, M. Barquins, *Tectonophysics*, **295**, 341 (1998).

19. D.A. Hills, D. Nowell, A. Sackfield, *Mechanics of Elastic Contacts*, Butterworth-Heinemann ltd Oxford 55-57 (1993).

20. J. Perez, *Physique et mécanique des polymères amorphes*, Technique et documentation-Lavoisier Paris 109 (1992).

21. S. Fouvry, P. Kapsa, H. Zahouani, L. Vincent, *Wear*, **203-204**, 393 (1997).

22. J. Geringer, B. Forest, P. Combrade, *Wear*, (2006) in press.

23. Y. Grohens, P. Carriere, J. Spevacek, J. Schultz, *Polymer*, **40**, 7033 (1999).

24. Y. Grohens, M. Brogly, C. Labbe, J. Schultz, *Eur. Polym. J.*, **37**, 691 (1997).

25. J. Brandrup, E.H. Immergut, E.A. Grulke, *Polymer Handbook*, John Wiley & Sons editors, Wiley-Interscience Publication New-York (1999).

Tables list

Elements	Cr	Ni	Mo	Mn	Si	Cu	C	P	S	Fe
Composition (% w/w)	17.05	14.55	2.80	1.80	0.40	0.10	0.02	0.02	<0.01	Bal.

Table 1. Chemical composition of 316L stainless steel.

Tacticity i/s/a (%)	Mn, average molecular weight number ($g.mol^{-1}$)	I, polydispersity index	η, intrinsic viscosity ($L.g^{-1}$)	Tg, glass transition temperature (K)
2/49/49	242090 ± 2500	1.51 ± 0.05	0.154 ± 0.04	393 ± 7

Table 2. Characteristics of the reference PMMA, without degradation; i/s/a: isotactic/syndiotactic/atactic.

Normal load F_n, ($N.mm^{-1}$)	Wear time coefficient α_V', ($\mu m^3.s^{-1}$)	Coefficient r^2 V = f(t)	Wear energy coefficient α_V, ($10^6 \mu m^3.J^{-1}$)	Coefficient r^2 V = f(E_{dc})
2.83	$7.6.10^2$	0.83	0.29	0.89
5.67	$5.6.10^2$	0.86	0.13	0.93
8.5	$6.1.10^2$	0.83	0.18	0.99
11,33	$4.5.10^2$	0.83	0.13	0.99

Table 3. Time and cumulated dissipated energy influence on the wear volume evolution. Wear time and wear energy coefficient, α_V' and α_V, are the slopes of the lines representing wear volume vs. time and cumulated dissipated energy respectively; coefficient r^2: correlation coefficient.

M ($g.mol^{-1}$)	α_v ($mm^3.J^{-1}$)	ρ ($g.mm^{-3}$)	φ_{mol} ($kJ.mol^{-1}$)	$D_{(C-C)}$ ($kJ.mol^{-1}$)	$\varphi_{mol}/D_{(C-C)}$
100	$1.8.10^{-4}$	$1.18.10^{-3}$	470810	350 (298 K)	1345

Table 4. Molar wear energy coefficient, comparison with the bond energy carbon-carbon. M: molar weight of monomer methylmethacrylate; α_V: wear energy coefficient; ρ: specific gravity; φ_{mol}: molar wear energy coefficient; $D_{(C-C)}$: bond energy of carbon-carbon.

E* (Pa)	b (m)	z (m)	w ($J.m^{-2}$)	θ	$D_{(C-C)}$ ($J.mol^{-1}$)	$D_{(C-C)}.\theta$ ($J.mol^{-1}$)	**α_V, theory ($mm^3.J^{-1}$)**	**α_V, experimental ($mm^3.J^{-1}$)**
$2.91.10^{9}$	$3.00.10^{-6}$	$7.5.10^{-8}$	$2.5.10^{-2}$	1380	$3.5.10^{5}$	$4.83.10^{8}$	**$1.75.10^{-4}$**	**$1.8.10^{-4}$**

Table 5. Comparison between the wear energy coefficient calculated with Fuller-Tabor parameter and the one obtained experimentally. $F_N = 5.67$ $N.mm^{-1}$.

Samples	T_g (°C)
1, PP	119 ± 7
2, PP	117 ± 7
3, PP	124 ± 7
4, PP	120 ± 7
5, PMMA fretting	128 ± 7

Final results

T_g = 120 ± 3 °C / T_g = 128 ± 7 °C

PMMA, polishing PMMA, fretting

Table 6. Glass transition temperatures, T_g, for two PMMA samples types, PP represents the polished PMMA, without fretting; PMMA fretting is a sample after a duration of 1,620,000 seconds.

a)

δ (ppm)	height (u,a)	config	%
1.554	1445172	isotactic	2
1.422	33817024	atactic	49
1.287	33780531	syndiotactic	49

b)

δ (ppm)	height (u.a)	config	%
1.172	2626197	isotactic	3
1.026	38385779	atactic	37
0.918	60352680	syndiotactic	60

Table 7. a) Reference PMMA configuration; b) debris of PMMA configuration; δ(ppm): NMR shift, u.a: arbitrary unit, height: height of the peak on NMR signal vs. NMR shift corresponding to the configuration, config: configuration.

Figures list

Fig. 17. Attenuated total reflection-FTIR spectrum of: a) reference PMMA; b) PMMA debris after fretting test, duration = 80,000 seconds, F_N = 8.5 N.mm^{-1}.

Fig. 18. Ratio between absorbance at 840 cm^{-1} and absorbance at 860 cm^{-1}, ATR-FTIR measurements on worn PMMA surface. For each number of cycles, the average value is obtained from four different normal loads.

Fig. 19. Scheme of the structure of helix and trans-gauche conformation on metal surface.

Figures

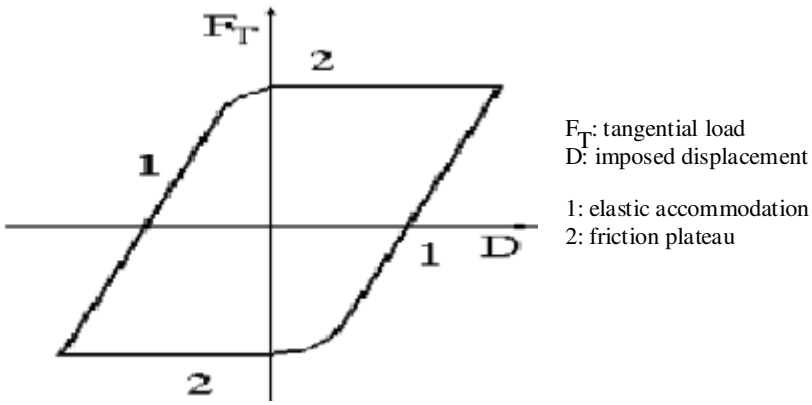

Fig. 1. Cycle $F_T = f(D)$, gross slip regime.

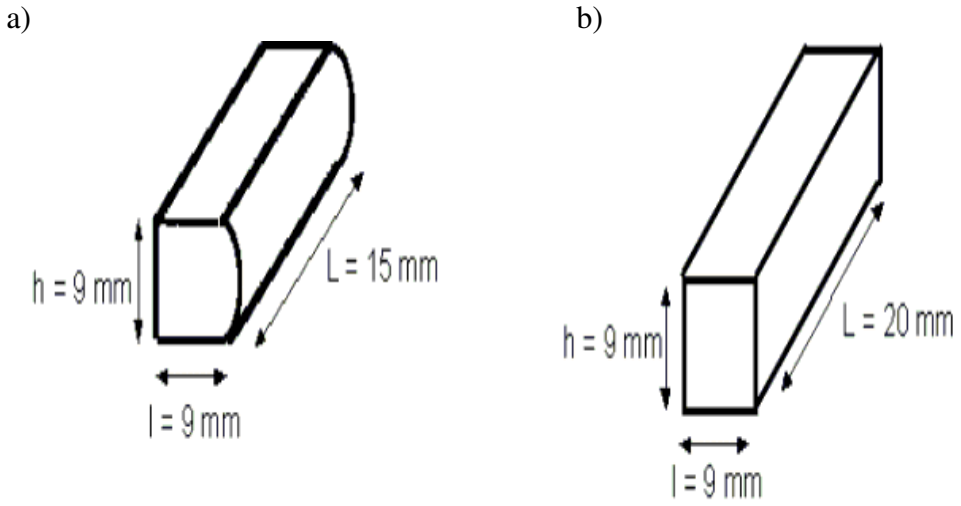

Fig. 2. Shape and dimensions of a) PMMA specimen, radius of curvature equal to 10 mm; b) 316L specimen.

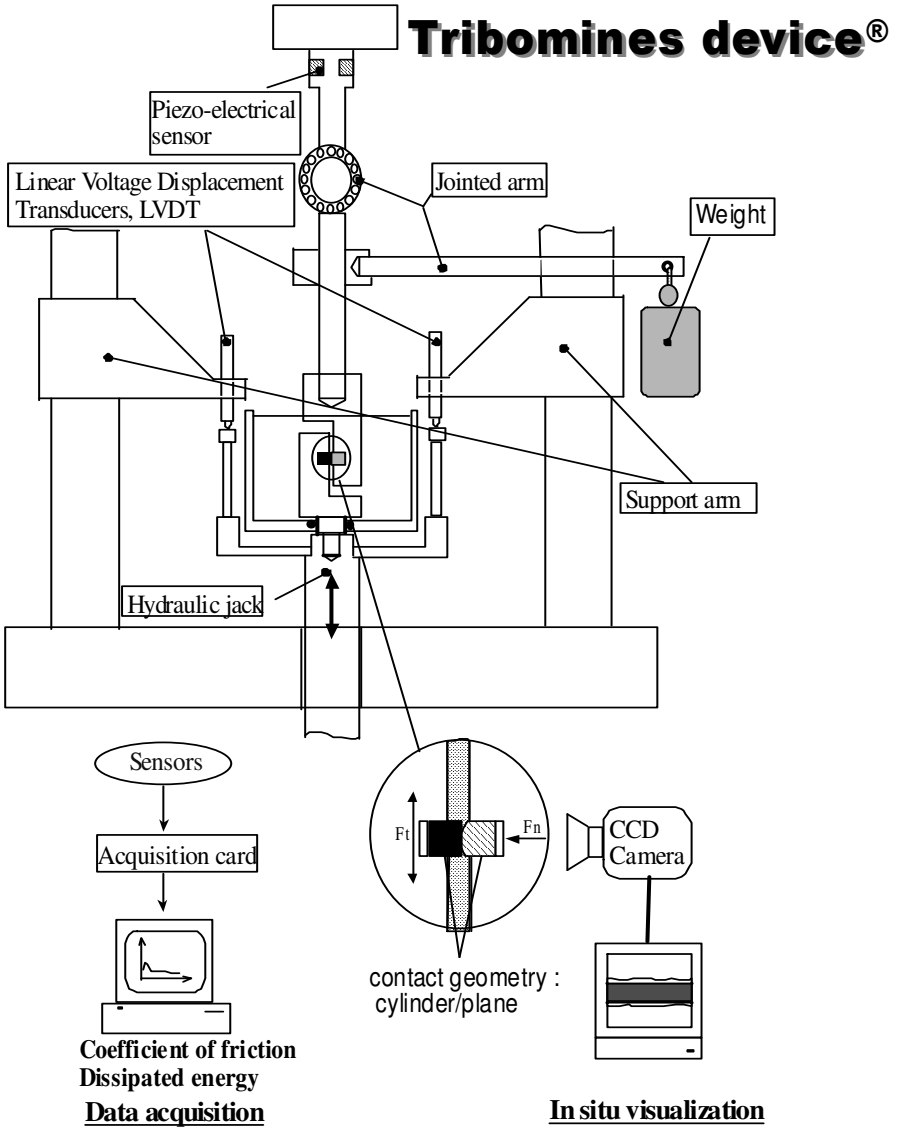

Fig. 3. Tribomines® experimental device.

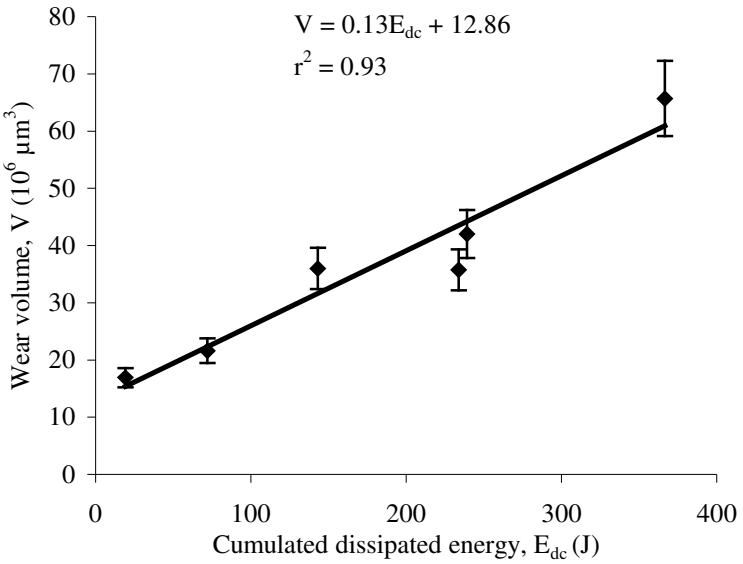

Fig. 4. Wear volume (10^6 µm^3) vs. the cumulated dissipated energy (J); F_N = 5.67 N.mm^{-1}; frequency = 1 Hz.

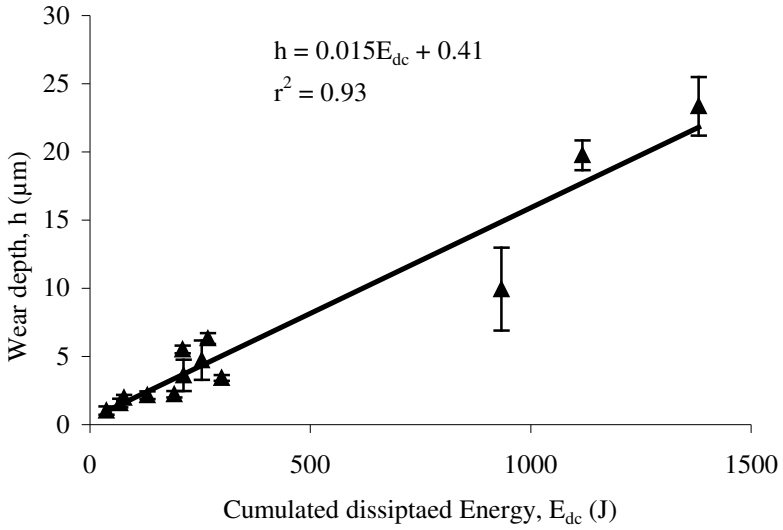

Fig. 5. Wear depth (µm) vs. the cumulated dissipated energy (J); F_N = 5.67 N.mm^{-1}; frequency = 1 Hz.

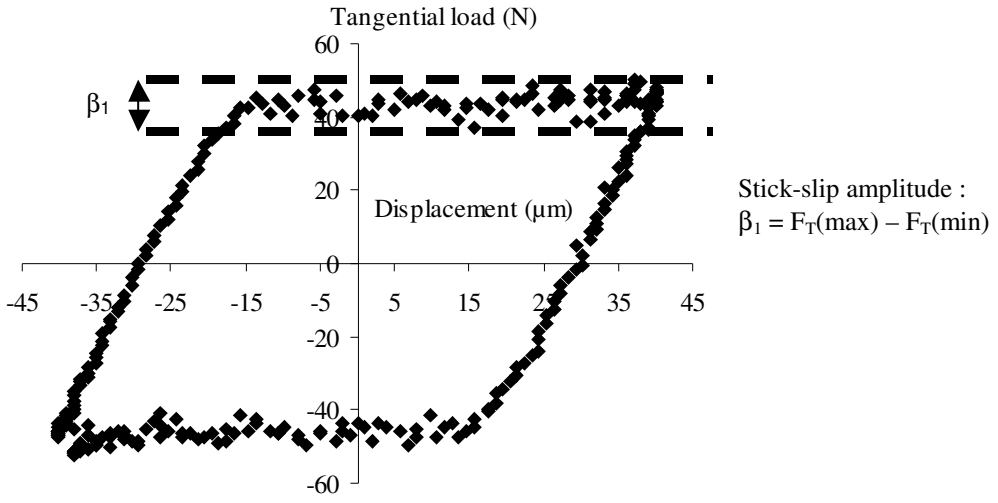

Fig. 6. Fretting cycle, tangential load vs. displacement, β_1 (N): stick-slip amplitude; F_N = 5.67 $N.mm^{-1}$, frequency = 1 Hz.

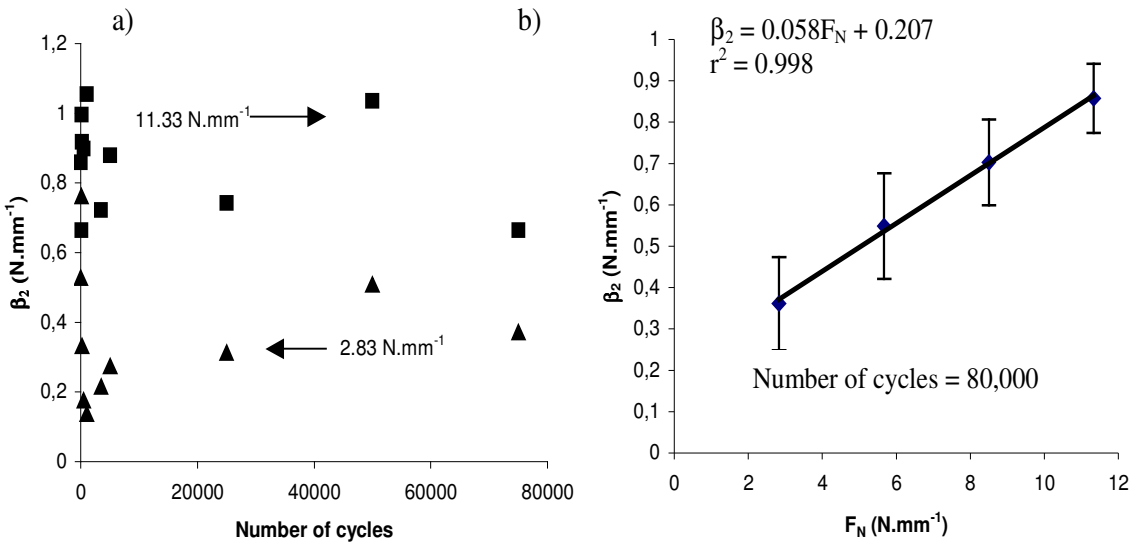

Fig. 7. a) Stick-slip coefficient, β_2, vs. number of cycles, frequency = 1 Hz, normal load is equal to 11.33 N.mm^{-1} (upper values) and 2.83 N.mm^{-1} (lower values); b) Average stick-slip coefficient, β_2, vs. normal load per contact length unit, F_N, the number of cycles = 80,000.

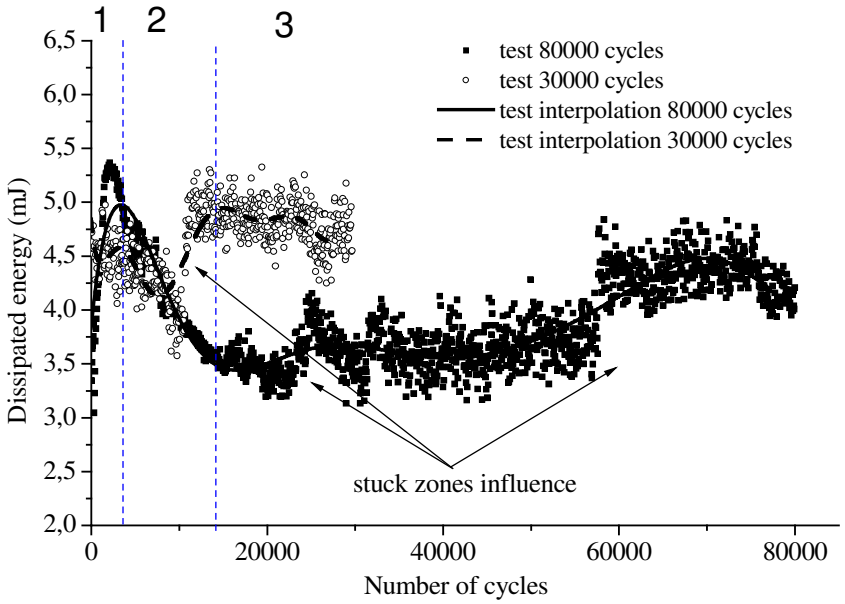

Fig. 8. Stuck zones influence, dissipated energy vs. number of cycles; F_N = 11.33 N.mm^{-1}, frequency = 1 Hz.

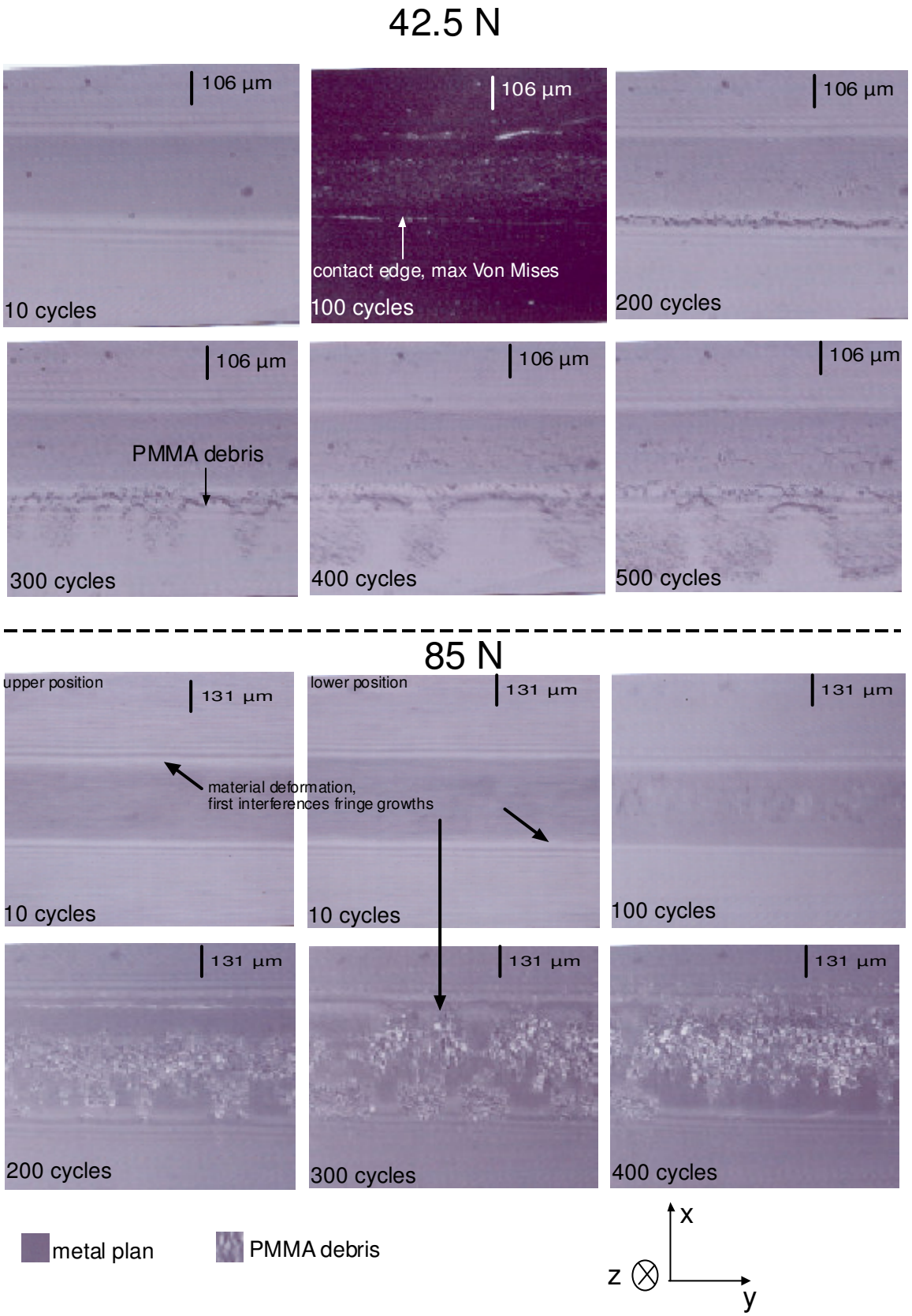

Fig. 9. 2D images of the contact 316L/PMMA; F_N = 2.83 N and 5.67 N.mm^{-1}, the number of cycles is within the range of 0 to 500 cycles.

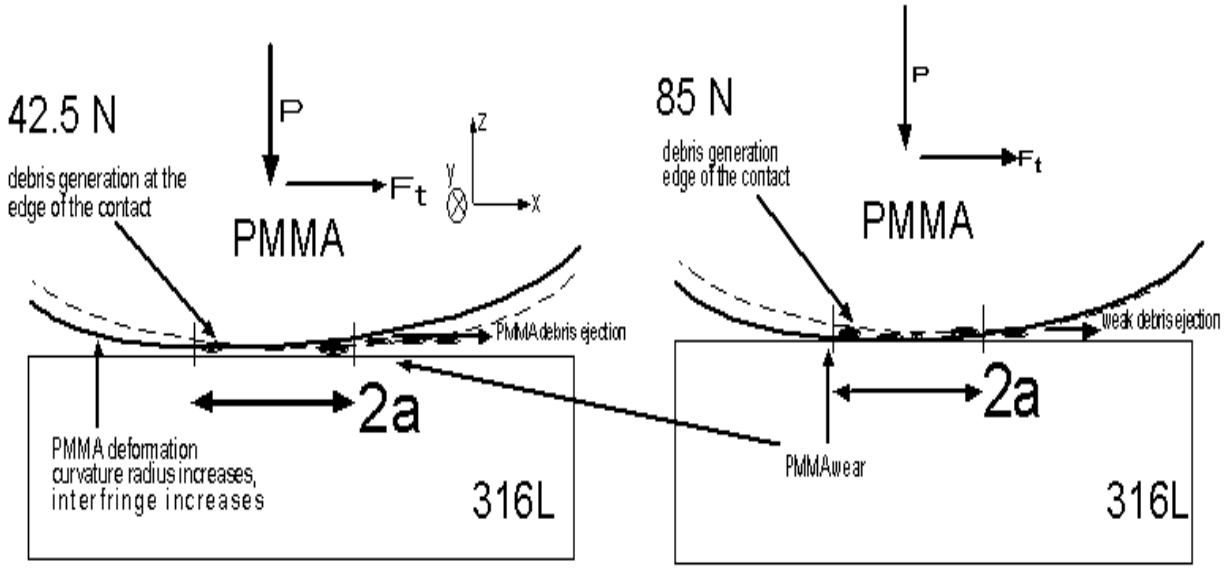

Fig. 10. Mechanisms of PMMA debris ejection according to the normal load, F_N = 2.83 $N.mm^{-1}$ and 5.67 $N.mm^{-1}$; a: semi contact width.

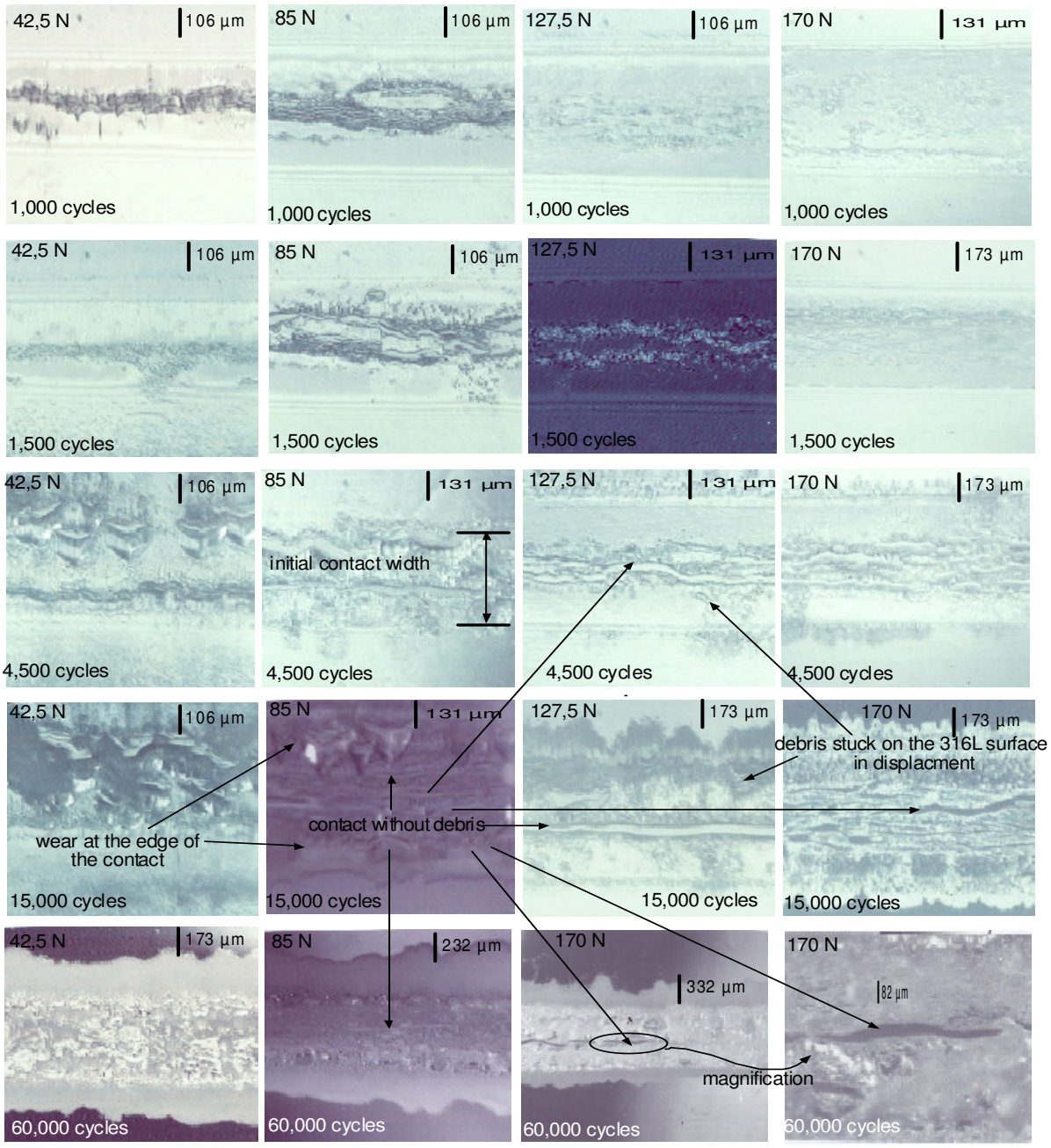

Fig. 11. 2D images of the contact 316L/PMMA; F_N = 2.83 N.mm^{-1} and 5.67 N.mm^{-1}, number of cycles is within the range of 1,000 to 60,000.

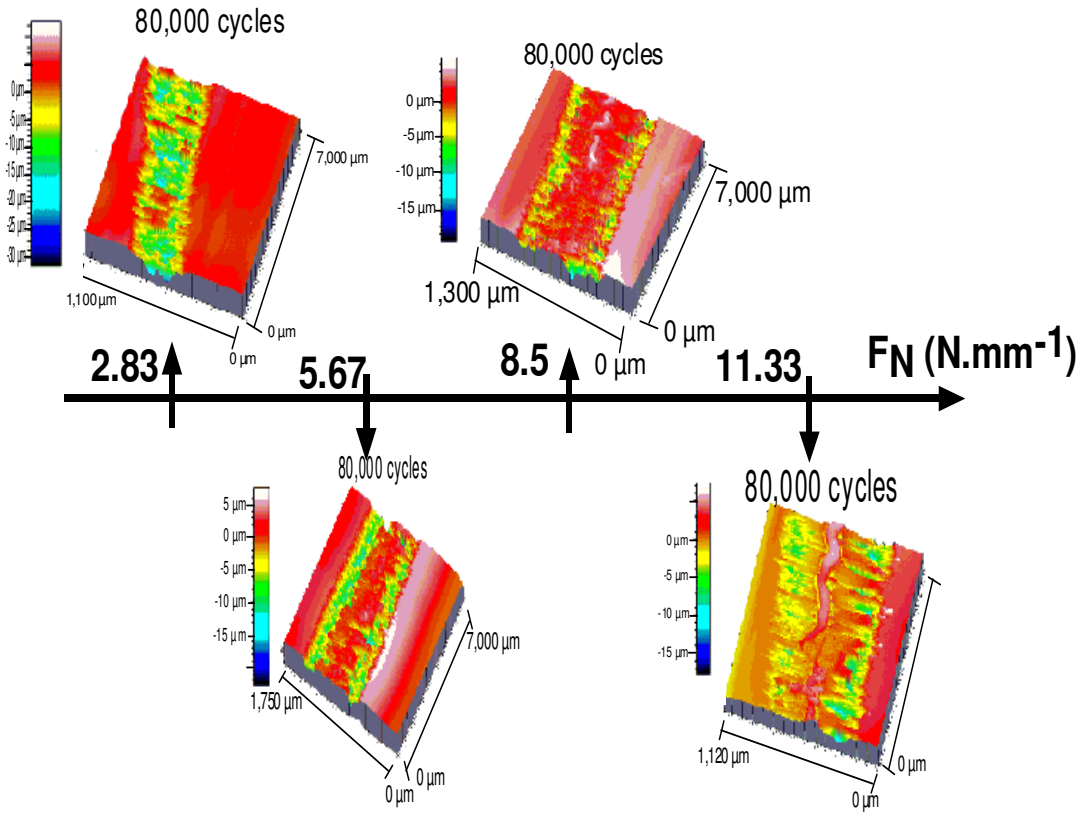

Fig. 12. PMMA 3D images from the contact 316L/PMMA; F_N within the range of 2.83 to 11.33 N.mm^{-1}, the number of cycles is equal to 80,000.

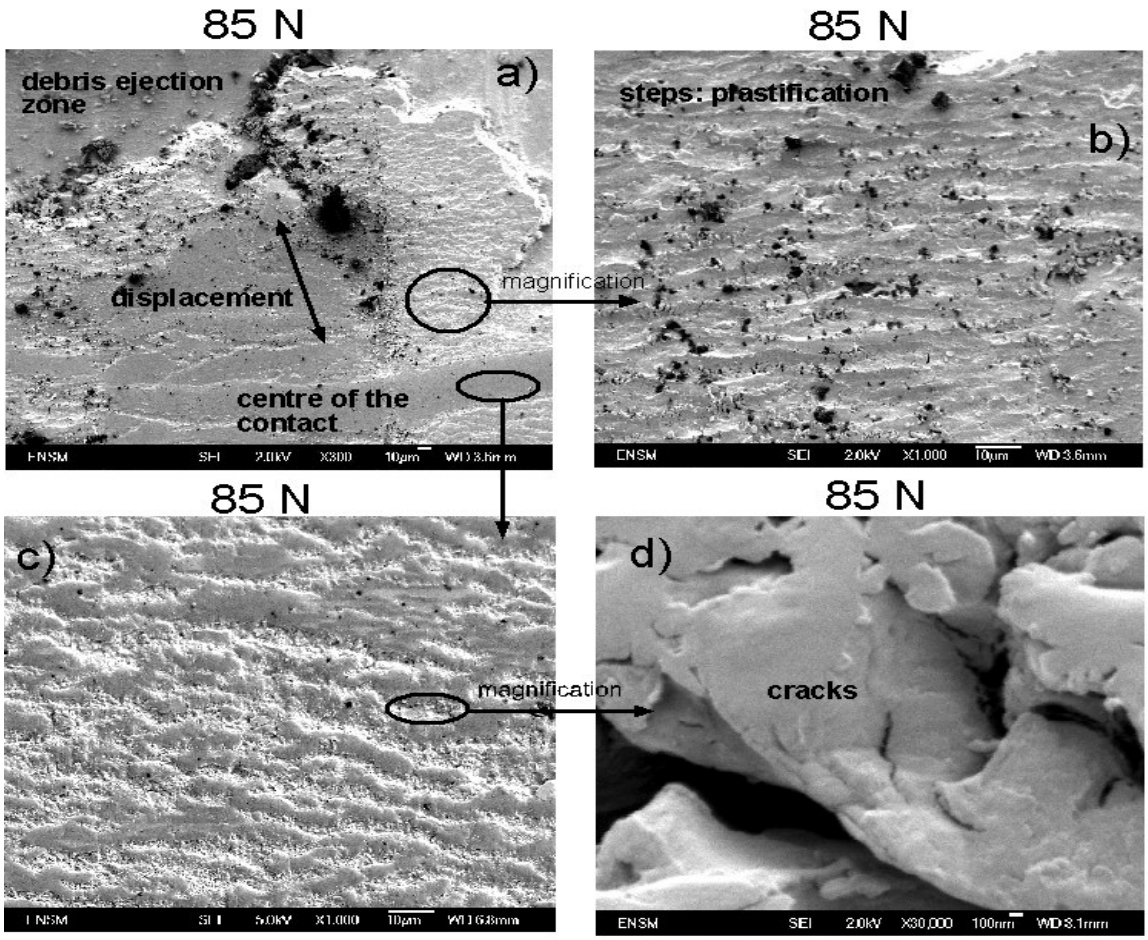

Fig. 13. SEM images of the PMMA; F_N = 5.67 N.mm^{-1}, number of cycles = 80,000.

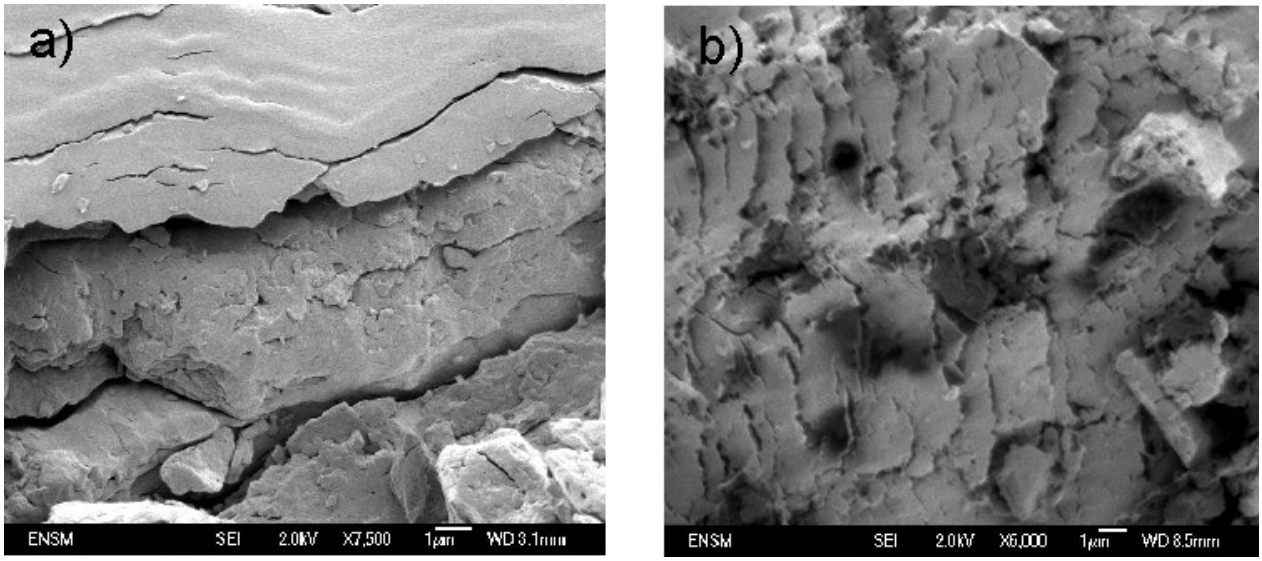

Fig. 14. SEM images of the PMMA; a) F_N = 2.83 N.mm^{-1} and b) 11.33 N.mm^{-1}.

a) b)

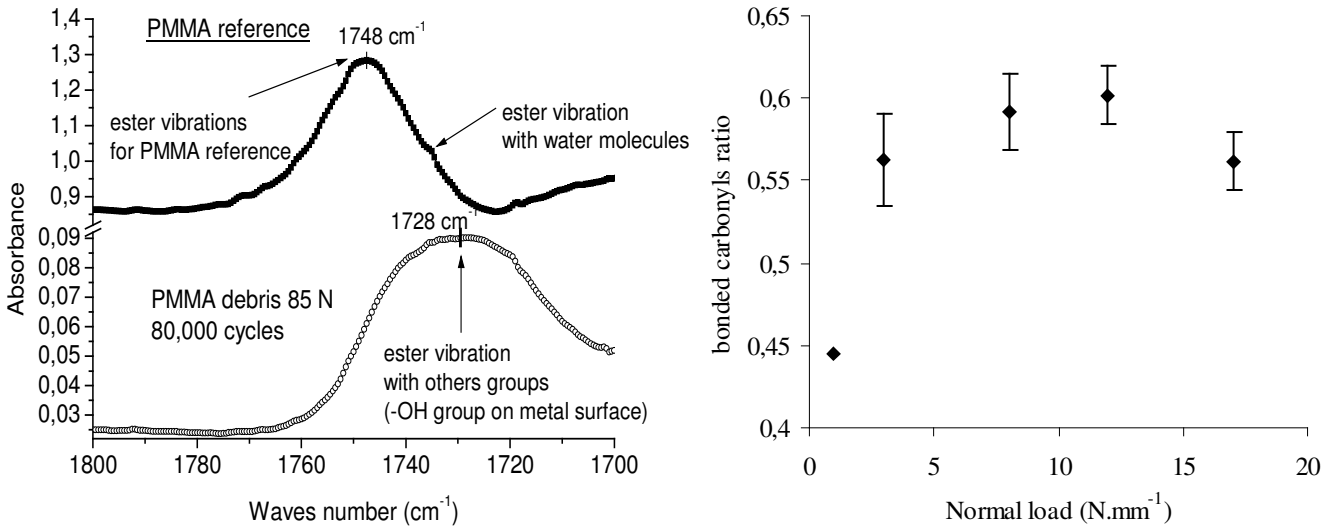

Fig. 15. a) Reflection-Absorption FTIR spectrum of PMMA reference sample, without fretting, and PMMA debris on metal surface, after fretting during 80,000 cycles, waves number within the range of 1800 to 1700 cm^{-1}; b) Bonded carbonyls ratio according to the applied normal load, accuracy calculated from five different spectra.

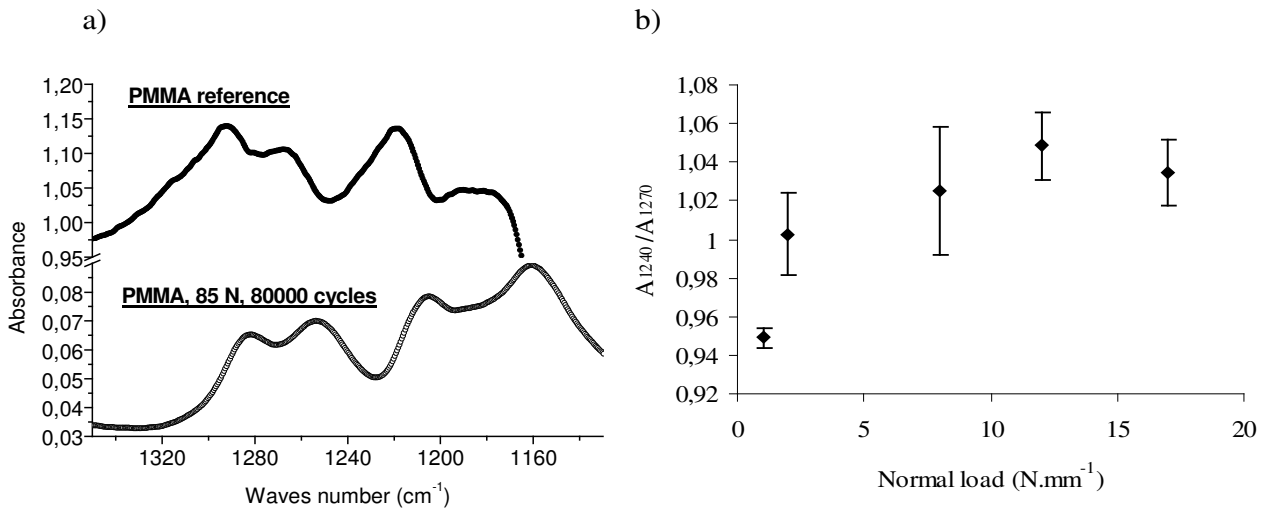

Fig. 16. a) Reflection-absorption IR spectrum of PMMA reference sample, without fretting, and PMMA debris on metal surface, F_N = 5.67 N.mm^{-1}, number of cycles = 80,000 cycles, waves number within the range from 1350 to 1150 cm^{-1}; stretching of the vibration C-O-CH_3; b) ratio of the absorbance A_{1240}/A_{1270}.

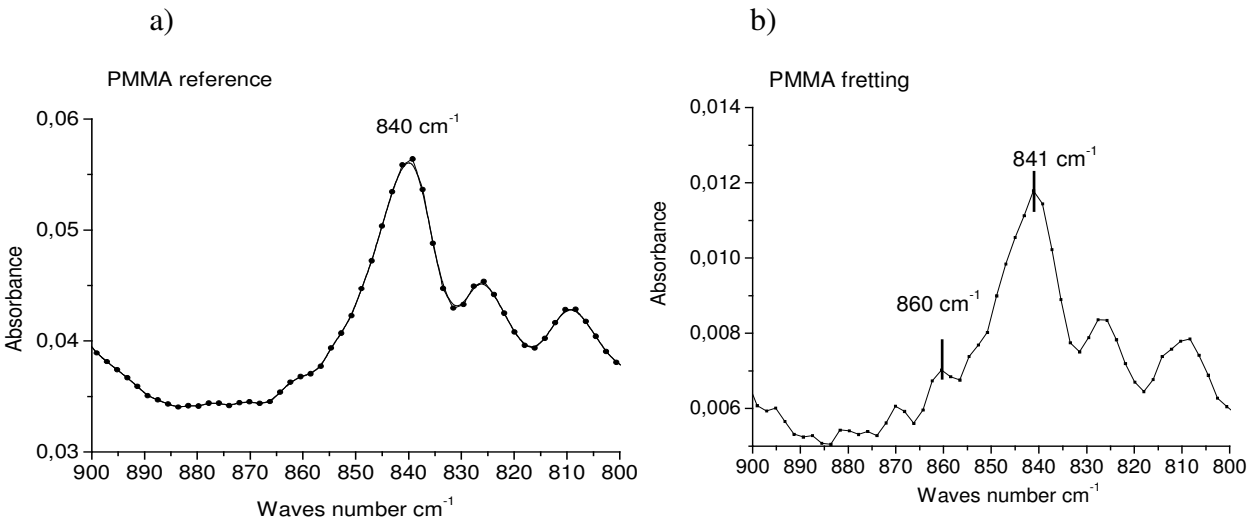

Fig. 17. Attenuated total reflection-FTIR spectrum of: a) reference PMMA; b) PMMA debris after fretting test, duration = 80,000 seconds, F_N = 8.5 N.mm^{-1}.

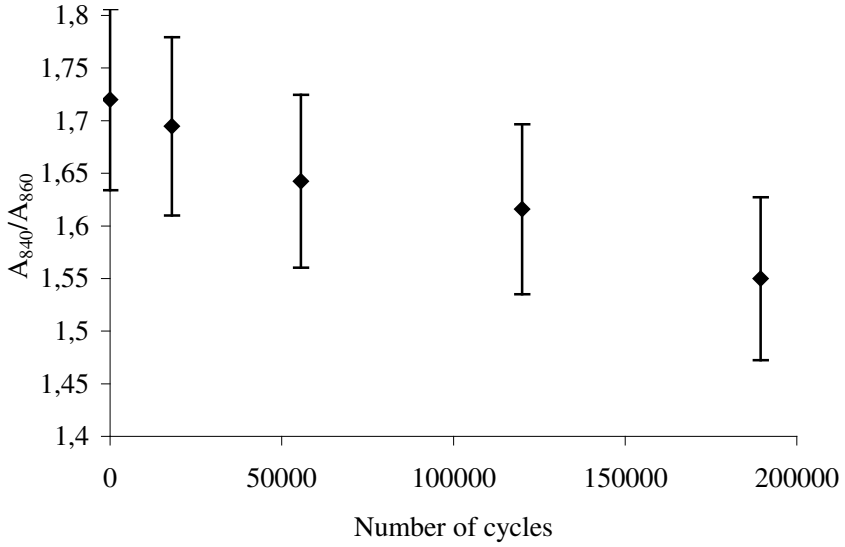

Fig. 18. Ratio between absorbance at 840 cm^{-1} and absorbance at 860 cm^{-1}, ATR-FTIR measurements on worn PMMA surface. For each number of cycles, the average value is obtained from four different normal loads.

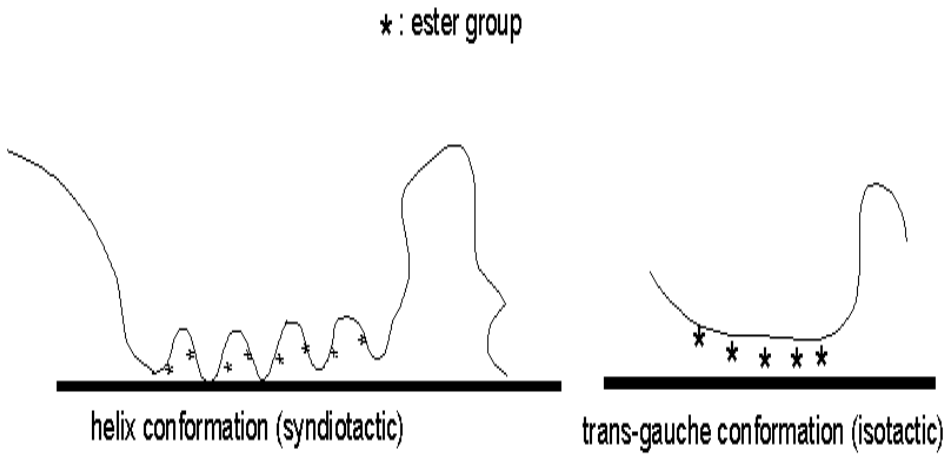

Fig. 19. Scheme of the structure of helix and trans-gauche conformation on metal surface.